A new stator windings design for brushless doubly fed machines

S Abdi*, R McMahon [†], E Abdi[ł]

**Faculty of Engineering Environment and Computing, Coventry University, Coventry, UK, Email:ac7019@coventry.ac.uk*
[†]Warwick Manufacturing Group (WMG), Warwick University, Coventry, UK
[ł]Wind Thechnologies Limited, St Johns Innovation Park, CB4 0WS, Cambridge, UK

Keywords: Brushless doubly fed machine (BDFM), finite element (FE) analysis, unbalanced magnetic pull (UMP), rotor eccentricity, parallel winding

Abstract

The Unbalanced Magnetic Pull (UMP) is intrinsically higher in a BDFM than a single field machine such as induction motors. This will be more exacerbated by the presence of rotor eccentricity, causing considerable amount of noise and vibration in the BDFM. This paper proposes new approaches for designing the stator windings in a BDFM, by connecting the appropriate stator coil groups in parallel in order to diminish the UMP and its resulting vibration. Parallel connections of stator coils may however lead to direct coupling of stator windings. The analytical methods presented in this study propose appropriate ways of paralleling the coils to avoid such problems. The effects of the use of parallel windings as a way to mitigate the UMP is then studied, using 2-D Finite element (FE) analysis, showing significant improvements.

1 Introduction

The brushless doubly-fed machine (BDFM), also known as the brushless doubly-fed induction generator (BDFIG), is an alternative to the well-established DFIG for use in wind turbines [1]. The BDFM retains the benefit of utilising a partially rated converter, but offers higher reliability, and hence lower cost of ownership, than the DFIG because of absence of brush gear and slip-rings [2]. In addition, the BDFM is intrinsically a medium-speed machine, enabling the use of a simplified one or two-stage gearbox; hence, reducing the cost and weight of the overall drivetrain and further improving reliability [3]. A schematic of the BDFM drivetrain is shown in Fig. 1.

To date, several groups have reported experimental BDFMs [1, 4-6] and there have been attempts to construct machines of higher power to confirm the machine's suitability for MW power applications [5, 6], but few details of machine design and performance have been published.

The modern BDFM concept as a variable speed drive or generator comprises two electrically separate stator windings, one connected directly to the mains, called the power winding (PW), and the other supplied from a variable voltage and frequency converter, called the control winding (CW). The pole numbers of the two stator windings are chosen so as to avoid direct coupling and a special rotor design is used to couple between the two stator windings, the nested-loop design being commonly used [1]. The machine therefore contains three magneto motive forces (MMFs), the first in the stator directly supplied from the mains, the second in the stator supplied from the converter and the third induced in the rotor. The normal mode of operation of the BDFM is as a synchronous machine with the rotor rotating at a speed determined by the winding pole numbers and the mains and converter frequencies.

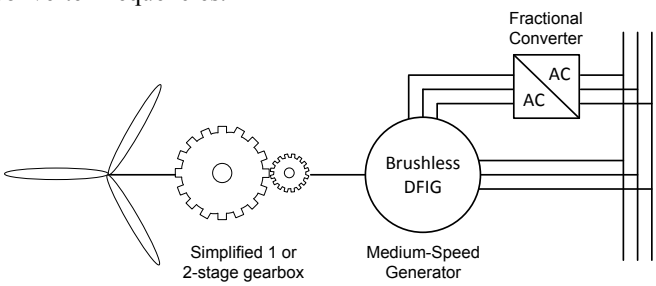

Fig. 1: BDFM drivetrain.

Fig. 2: 250 kW D400 BDFM (right front) on test bed.

As with all induction type machines, characterized by relatively small air gaps, the strong magnetic fields across the air gap exert considerable forces on the iron parts of the machine. These cause time-varying deflections on the machine surface which lead to vibration and acoustic noise. One source of producing deflection is unbalanced magnetic pull (UMP), which can be mathematically shown as the interaction between

two air gap flux waves with pole-pair numbers differing by one [7].

The presence of rotor eccentricity in practical machines further modulates the field patterns, exacerbating the resulting vibration. An eccentric rotor motion occurs when the rotor axis is not aligned with the axis of the stator bore. Due to manufacturing tolerances, wear of bearings, and other reasons, some degree of rotor eccentricity is always present. Static UMP is caused by the rotor axis being positioned parallel to, rather than being on, the stator axis as a result of manufacturing tolerances. In this case, the rotor is rotating around its own axis. Dynamic UMP occurs when the rotor is precessing about the stator bore center but not its own center.

Parallel connection of stator coils is widely used to reduce UMP in electrical machines with non-uniform air gaps and its effects have been discussed in the literature, for example in [8]. Effectively, the variation of reluctance due to uneven air gap length causes circulating currents in the parallel paths, which improve the air gap flux distribution, hence reducing the deflection and UMP.

The effects of rotor eccentricity on machine performance and the use of parallel windings, as a way to suppress its effects, have been studied for induction machines [11–13], synchronous machines [14], switched reluctance machines [15] and permanent magnet machines [16]. But little work has been done on UMP and vibration analysis for the Brushless Doubly Fed Induction Machine (BDFIM) [17, 18] and Brushless Doubly Fed Reluctance Machine (BDFRM) [19]. Connecting the stator coils in parallel in a BDFM is not as straightforward as in other electrical machines. The main reason is that parallel connection of stator coils may lead direct coupling of stator windings if not considered carefully. The large circulating currents produced by direct coupling will cause significant losses and degrade machine performance.

A detailed study of UMP and its resultant displacement in stator back iron for the BDFM is presented in this paper taking the effects of rotor eccentricity into account. The key contribution of this paper is the assessment of the parallel connection of stator coils in the BDFM such that direct coupling is eliminated. This is particularly challenging when short pitched windings are used.

2 Prototype machine considered in this study

The specifications of the 250kW D400 BDFM are shown in Table 1. The D400 BDFM was constructed as a frame size D400 machine with the stack length of 820 mm. The stator windings were form wound from copper strips. The power winding was rated at 690 V, 178 A, at 50 Hz and the control winding was designed for 620 V at 18 Hz and rated at 73 A. Both stator windings were connected in delta. The rotor comprises six sets of nests each consisting of a number of concentric loops [20], the conductors being solid bars with one common end ring [21]. The magnetic properties for the iron were provided by the machine manufacturer. The D400 BDFM on test bed is shown in Fig. 2.

Frame size	400
PW pole number	4
PW rated voltage	690V at 50 Hz (delta)
PW rated current	178 A (line)
CW pole number	8
CW rated voltage	620 V at 18 Hz (delta)
CW rated current	73 A (line)
Speed range	500 rpm ± 36%
Rated torque	3670 Nm
Rated power	250 kW at 680 rpm
Efficiency (at full load)	> 95%
Stack length	0.82 m

Table 1: Specifications of the 250kW D400 BDFM

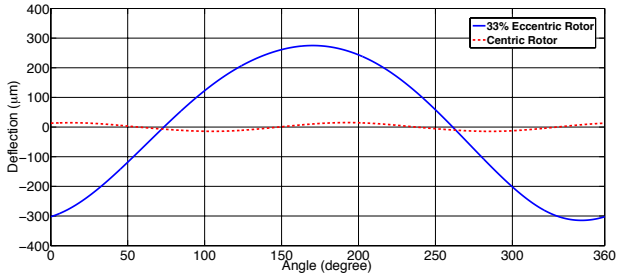

Fig. 3: Displacement in the stator back iron when the rotor is centric and when the rotor is 33% eccentric

3 Magnetic forces and resulting deflection

The radial forces exerted by the air gap magnetic field on the stator tooth tops are calculated. The effect of tangential forces on the teeth which ultimately exert torque to the machine's shaft are not considered in this analysis [9]. The air gap magnetic field is essentially the superposition of two field components, one with $2p_1$ poles, the mean absolute flux density of $\bar{B}_1$ rotating at ω_1 rad/s and another with $2p_2$ poles, $\bar{B}_2$ flux density rotating at ω_2. The total flux density as a function of space angle and time is therefore:

$$B(\theta,t) = \frac{\pi}{2}[B_1\cos(p_1 + \omega_1 t + \phi_1) + B_2\cos(p_2 + \omega_2 t + \phi_2)] \quad (1)$$

where ω_1 and ω_2 are the frequencies of the two stator supplies, and, ϕ_1 and ϕ_2 are phase offsets. Any harmonic field components created by the rotor structure, slotting, saturation and rotor eccentricity are ignored in (1). In Fig. 4, a typical air gap field for a 4/8 pole BDFM at the point where t and ϕ terms are zero is shown in black, i.e. the smooth line. The field represents magnetic loading of 0.48 T, which is the design value for the 250 kW BDFM. The air gap flux density obtained from 2-D linear FE modeling which takes into account all the harmonic components mentioned above is also shown in Fig. 4 for a centric rotor. The magnetic field in the

air gap exerts an inward force on the stator tooth top and an equal and opposite outwards force on the rotor tooth tops. At any point the force is related to the magnetic field strength by [21]

$$f = \frac{B^2(\theta,t)}{2\mu_0} \quad (2)$$

This force will cause the stator back iron to deflect, which is estimated using 1-dimensional beam theory as proposed by Alger [22]. The force must be balanced by elastic deformation of the back iron and the frame. The force in the air gap may be replaced by an equivalent force at the central axis of the back iron (the dashed line in Fig. 3) given as a function of the mechanical angle by

$$f_b(\theta,t) = \frac{D_a}{D_c}\frac{B^2(\theta,t)}{2\mu_0} \quad (3)$$

where D_a is the air gap diameter and D_c is the diameter at the center of the back iron. The force can be considered as the superposition of two components, the average force, which causes a small deflection constant in θ and can be neglected [8], and the space varying component given by

$$f_b'(\theta,t) = f_b(\theta,t) - \frac{1}{2\pi}\int_0^{2\pi} f_b(\theta,t).d\theta \quad (4)$$

Next, the deflection resulted from this applied force can be calculated. The force is resisted mainly by the stator back iron, as the machine's frame makes negligible contribution to resisting the magnetic forces due to its much lower bending stiffness [8]. The shear stress S in the beam is related to the force by

$$S(\theta,t) = \frac{D_c l}{2}\int f_b'(\theta,t).d\theta \quad (5)$$

The shear stress is the differential of the bending moment, M and therefore

$$M(\theta,t) = \frac{D_c}{2}\int S(\theta,t).d\theta \quad (6)$$

Finally the deflection, $v(\theta,t)$ due to the loading is given by the double integral of the bending moment

$$v(\theta,t) = -\frac{D_c^2}{4}\frac{12}{E_{ym} l y_c^3}\int\int M(\theta,t).d\theta \quad (7)$$

where E_{ym} is the Young's Modulus of the material, y_c is the core back depth and l is the stator stack length. In the present study, the air gap flux density, $B(\theta,t)$, is obtained from FE modeling. Then from (2) to (7), the stator back iron displacement is obtained. Fig. 3 shows the resulting deflections in stator back iron when the rotor is statically eccentric by 33%, and when the rotor is centric. As it is obvious, the deflection level in the presence of rotor eccentricity is significantly i.e. 18 times larger than the case of an ideally constructed machine. Therefore, the mitigation of UMP is important in the BDFM if standard manufacturing tolerances are allowed.

4 Stator parallel windings in brushless doubly fed machines

Paralleling the stator coils is a well-known practice to mitigate UMP in electrical machines caused by a non-uniform air gap. In the BDFM, the pole pair numbers for the PW and CW are typically chosen in a way that when their coils are connected in series, the net voltage in each phase of the PW and CW induced by direct coupling with the other winding's field is zero. Parallel connection of stator coils specially when short pitched windings are used can potentially lead to direct coupling between the two stator windings and hence, special care must be taken into account in the winding design. The induced voltage due to direct coupling of stator windings is calculated in the following section to assess various parallel winding designs.

4.1 Induced voltage due to direct coupling

Two principle fields are generated in the BDFM air gap when the PW and CW are supplied with three-phase balanced voltages. They are given, when the rotor is stationary, by

$$B_{PW}(\theta,t) = \bar{B}_{PW}\cos(\omega_{s1}t - p_1\theta) \quad (8)$$

$$B_{CW}(\theta,t) = \bar{B}_{CW}\cos(\omega_{s2}t - p_2\theta) \quad (9)$$

where ω_{s1} and ω_{s2} are the PW and CW angular frequencies respectively, θ is the angle expressed in a coordinate reference frame fixed to the rotor, and p_1 and p_2 are the PW and CW pole pair numbers, respectively. The magnetic flux linked by a single stator coil is obtained by

$$\phi = l\frac{d}{2}\int_{\alpha 1}^{\alpha 2} B(\theta,t).d\theta \quad (10)$$

where l is d are the lamination stack length and mean air gap diameter respectively. α_1 and α_2 are the angles representing the coil locations. From Faraday's law, the voltage induced in a single CW coil due to the p_1-pole air gap field is:

$$v_{coil}^{CW} = -N_{CW}\frac{d\phi_{PW}}{dt} = \frac{l d \bar{B}_{PW}\omega_{s1}}{2p_1}N_{CW}[\cos(\omega_{s1}t - p_1\alpha_2) - \cos(\omega_{s1}t - p_1\alpha_1)] \quad (11)$$

Fig. 4: Stator PW Short pitched by three slots

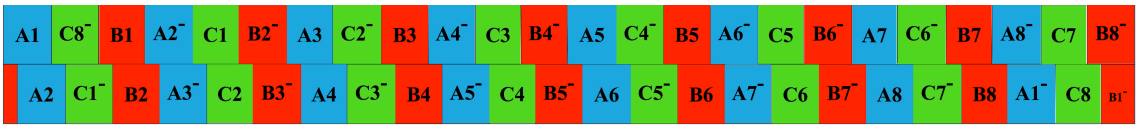

Fig. 5: Stator CW short pitched by one slot

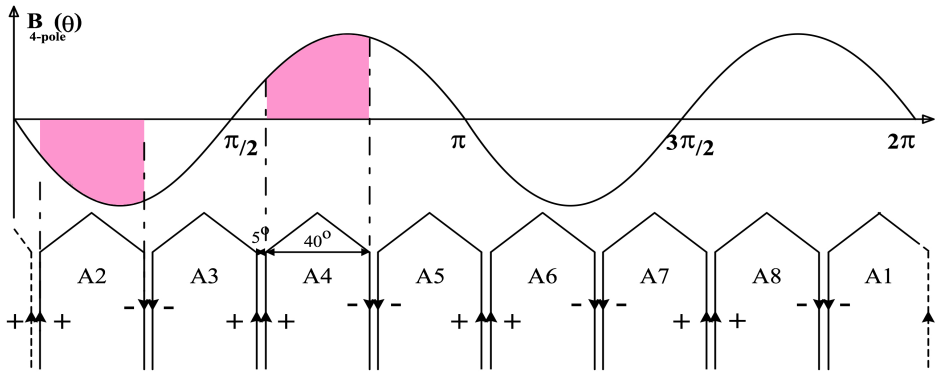

Fig. 6: 4-pole air gap field produced by the PW in the air gap, and the positions of CW coil groups. Series connection of coils A2 and A4 leads to zero net direct coupling

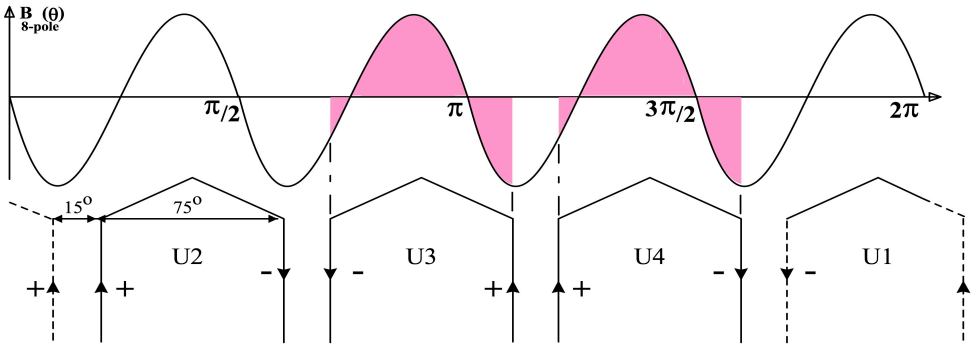

Fig. 7: 8-pole air gap field produced by the CW in the air gap, and the positions of PW coil groups. Series connection of coils U3 and U4 leads to zero net direct coupling

Similarly, the induced voltage in a single PW coil due to the p_2-pole air gap field is:

$$v_{coil}^{PW} = \frac{ld\bar{B}_{CW}\omega_{s2}}{2p_2} N_{PW}[\cos(\omega_{s2}t - p_2\alpha_2) - \cos(\omega_{s2}t - p_2\alpha_1)] \quad (12)$$

N_{PW} and N_{CW} are the number of PW and CW coil turns. The winding diagrams for the PW and CW in the 250 kW BDFM are shown in Figs. 4 and 5. Each colored area comprises a number of slots containing coils of a single phase. The coils of each phase located in adjacent slots of a single winding layer are connected in series, creating a coil group. This is normal practice in the majority of winding configurations. Each colored area i.e. X_i and $\bar{X}_i$ in Figs. 4 and 5 therefore represents a coil group. The PW has four coil groups per phase, each with six series-connected coils and the stator CW has eight coil groups per phase, each with three series-connected coils. Therefore, the induced voltages across the m*th* PW coil group, v_{Um}^{PW} and n*th* CW coil group, v_{An}^{CW} are:

$$v_{Um}^{PW} = \sum_{i=1}^{6} v_{U_m - i^{th}coil}^{PW} \quad (13)$$

$$v_{An}^{CW} = \sum_{i=1}^{3} v_{A_n - i^{th}coil}^{CW} \quad (14)$$

If the net induced voltage in a coil group from direct coupling with the other stator field, i.e v_{Um}^{PW} or v_{An}^{CW} is not zero, then sufficient number of coil groups must be connected in series to make the net sum to zero, hence eliminating the effect of direct coupling.

4.2 Parallel connection of coil groups when both PW and CW are short pitched

Stator winding short pitching is widely used in electrical machines with double-layer winding construction. Short pitching reduces the harmonic content of the flux density in the air gap and consequently produces a more sinusoidal current linkage distribution than a full-pitch winding [22]. Most of the BDFMs built by the authors and others including the 250 kW BDFM have employed short-pitch windings, as shown in Figs. 4 and 5.

However, the short pitch configuration causes each coil group to couple to the other stator field. But, series connection of all coil groups within a phase leads to a zero net induced voltage. With careful consideration, only the minimum number of coil

groups can be connected in series to produce a net zero induced voltage from the other stator field. Then, these series connected coil groups can be connected in parallel without causing any direct coupling. Equations (13) and (14) are used to calculate the induced voltage in PW and CW coil groups and following results are obtained:

$$v_{U1}^{PW} = v_{U3}^{PW} = -v_{U2}^{PW} = -v_{U4}^{PW} \quad (15)$$

$$v_{A1}^{CW} = v_{A5}^{CW} = -v_{A3}^{CW} = -v_{A7}^{CW} \quad (16)$$

$$v_{A2}^{CW} = v_{A6}^{PC} = -v_{A4}^{CW} = -v_{A8}^{CW} \quad (17)$$

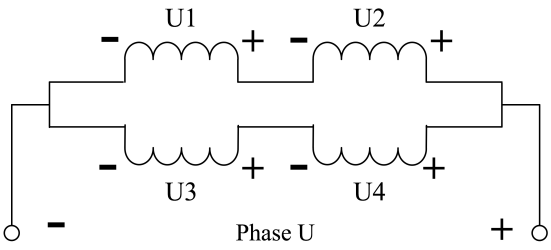

Fig. 8: Proposed connection of PW coil groups shown in Fig. 4, which eliminates the effect of direct coupling

From (15), (16) and (17), the PW coils can only be connected in parallel as shown in Fig. 8, but CW coils can have either of the arrangements shown in Fig. 9. The winding design shown in Fig. 9 (a) for the CW is expected to be more effective in reducing deflection since it contains more parallel paths.

Though the winding connections proposed in Figs. 8 and 9 for the PW and CW will eliminate direct coupling between the stator windings, they may still have a strong net coupling with the undesirable harmonics of the rotor field, making them impractical. It will be shown in the following section that the CW connection proposed in Fig. 9(a) will suffer from this issue.

4.3 Undesirable time harmonics in stator windings due to rotor harmonics

The 250 kW BDFM is modeled in FE in the synchronous mode of operation where its PW and CW are wound according to Figs. 8 and 9 (a) respectively. The rotor is perfectly constructed and the PW and CW are supplied at their rated voltages and frequencies, shown in Table I. Significant quantities of time harmonics is found in the CW currents when the machine reaches the steady state condition, as shown in Fig. 10. The largest harmonic is at 115 Hz with an amplitude of 48% of the main harmonic i.e. 15 Hz. This is caused by the coupling between undesirable rotor field harmonics and the CW coil groups, producing induced voltages that are not summed to zero through the proposed winding connection in Fig. 9 (a). The extent of stator current harmonic content can be found by evaluating the winding factor (*Kw*). *Kw* is affected by the winding configuration, and whether it is fully pitched or short pitched. In general, short-pitched winding structures lead to more sinusoidal stator currents [22]. FE analysis reveals that rotor time harmonics are present and Fig. 11 shows the Fast Fourier Transform (FFT) of current harmonics in rotor loops. Suppose the rotor current harmonic with the frequency of f_r^i can produce a rotor magnetic field with p_r^j pole pair number, then the speed of this field with respect to the rotor frame is:

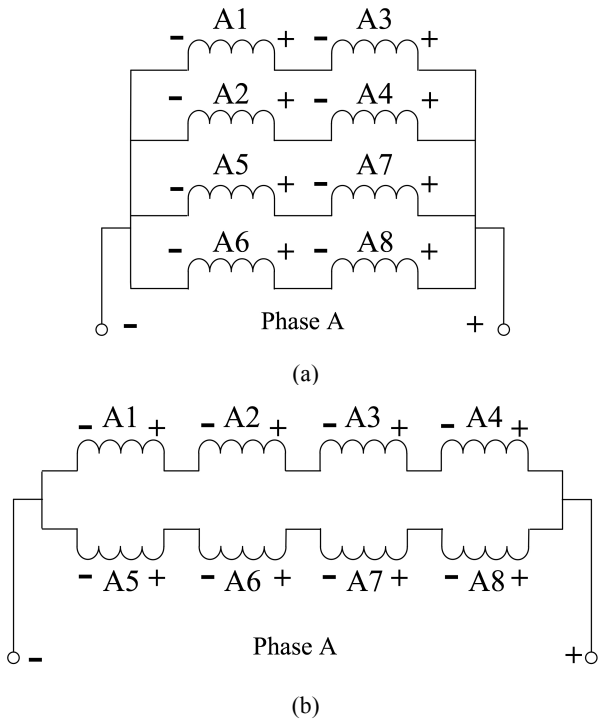

Fig. 9: Two proposed connections of CW coil groups shown in Fig. 5 which eliminate the effects of direct coupling

$$n_{B_r}^{rot(i,j)} = \frac{f_r^i \times 60}{p_r^j} \quad (18)$$

in *rpm*. The stator however sees this field with the speed of

$$n_{B_r}^{st(i,j)} = n_{B_r}^{rot(i,j)} \pm n_r \quad (19)$$

where n_r is the rotor shaft speed. If a stator coil couples with this field, the frequency of the induced current will be

$$f_{st}^{(f_r^i, p_r^j)} = n_{B_r}^{st(i,j)} \frac{p_r}{60} = f_r^i \pm p_r^j \frac{n_r}{60} \quad (20)$$

Using (20) and from the frequency of the current harmonics in a stator coil, the possible combinations of f_r^i and p_r^j can be obtained.

As shown in Fig. 10, the CW currents have a strong 115 Hz harmonic component. Using (20), the possible combinations of f_r^i and p_r^j are shown in Table 2. It should be noted that not all of these combinations are realistic. The nested-loop rotor produces various space harmonics, including $p_1, p_2, p_1 + nN_r$ and $p_2 + nN_r$, where N_r is the number of rotor nests and is an integer [23]. Therefore, among the possible combinations given in Table 2, only 4, 8, 16, 20, 32 and 56 pole-pairs exist.

Equations (11) to (14) can also be used to calculate the induced voltages in the CW coils when they are exposed to rotor magnetic field with pole numbers and frequencies given in Table 2. The following results are obtained for Cases 1 and 2:

$$v_{A1}^{CW} = v_{A2}^{CW} = \cdots = v_{A8}^{CW} \quad (21)$$

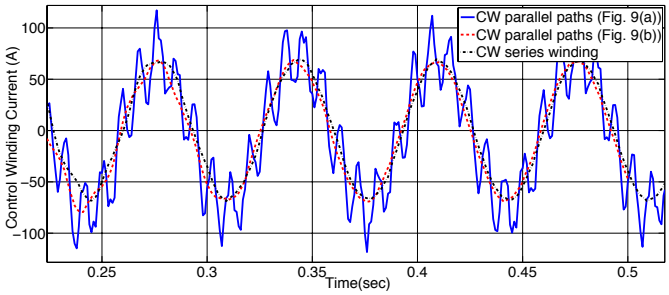

Fig. 10: Comparison of CW currents when its coils are connected in series, according to Figs. 9(a) and 9(b)

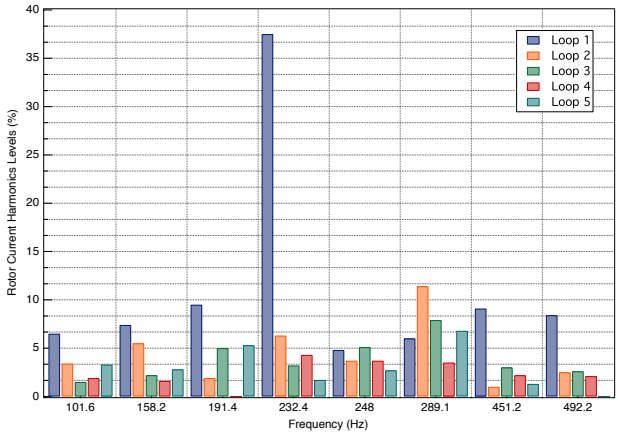

Fig. 11: FFT analysis of current harmonics in rotor loops. The amplitudes are expressed as percentage of the principle harmonic, i.e. 28.3 Hz in each loop.

and for Cases 4, 5, 6 and 8:

$$v_{A1}^{CW} = v_{A3}^{CW} = -v_{A2}^{CW} = -v_{A4}^{CW} \quad (22)$$

$$v_{A5}^{CW} = v_{A7}^{CW} = -v_{A6}^{CW} = -v_{A8}^{CW} \quad (23)$$

From (21) to (23) it can be shown that the CW design shown in Fig. 9 (a) shows a net coupling to the rotor field harmonics and hence is not a practical design. However, the PW and CW winding designs shown in Figs. 8 and 9 (b) do not couple to each other directly and to the rotor undesirable harmonic fields. The CW current for the winding design of Fig. 9 (b) is shown in Fig. 10 and as can be seen, does not contain significant harmonics.

5 Results and discussions

Different levels and types of rotor eccentricity are studied as described in Table 3. The back iron displacement for static and dynamic eccentricities are shown in Figs. 12 and 13, respectively, for series and parallel connected short pitched windings. The *rms* value of the deflection and its reduction as the result of parallel windings for different eccentricity types and levels are shown in Tables IV.

Case	1	2	3	4	5	6	7	8
f_r^i(Hz)	28	102	158	191	232	288	450	492
p_r^j	8	20	4	7	32	16	31	56

Table 2: Possible combinations of rotor current harmonics and the resulting field pole pair numbers producing a 115 Hz current harmonic in the CW.

Acronym	Eccentricity	Connections	
		PW	CW
C-SW	Centric	Series	Series
C-PW	Centric	Fig. 7	Fig. 8 (b)
SE-SW	Static	Series	Series
SE-PW	Static	Fig. 7	Fig. 8 (b)
DE-SW	Dynamic	Series	Series
DE-PW	Dynamic	Fig. 7	Fig. 8 (b)

Table 3: Different designs considered in this study

Significant reduction can be observed in the stator back iron displacement when parallel windings are employed. As shown in Tables 3, a reduction of between 55% to 80% in the displacement from static eccentricity can be achieved using parallel winding designs. The level of reduction is between 40 to 80 % for dynamic eccentricity.

6 Conclusion

This paper has studied the practicality of parallel winding designs in the BDFM such that the direct coupling between the two stator windings and with undesirable rotor field harmonics are eliminated. This is particularly important when short-pitched windings are utilized. It has been shown that with appropriate connection of coil groups in series and parallel, direct coupling of stator windings can be removed. There may be several possibilities of practical parallel winding designs, in which case the design with more parallel paths is shown to have stronger effect in suppressing the UMP.

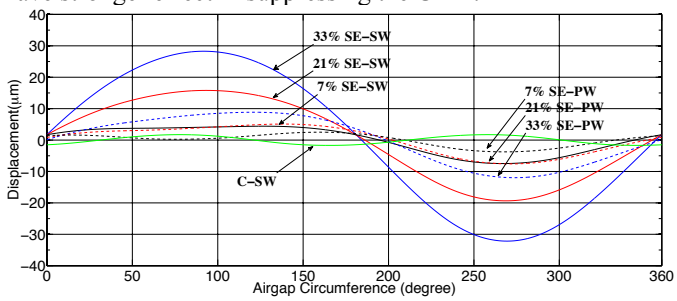

Fig. 12: Stator back iron deflection for different levels of rotor static eccentricities

Larger scale BDFMs are likely to be designed for slower natural speeds, hence with higher stator pole numbers. This will provide more possibilities for parallel connection of stator coils, but the practicality of such designs must be carefully assessed. The study presented in this paper, though is shown for a specific BDFM with 4 and 8 pole stator windings and a nested loop rotor, can be generalized for other BDFM designs.

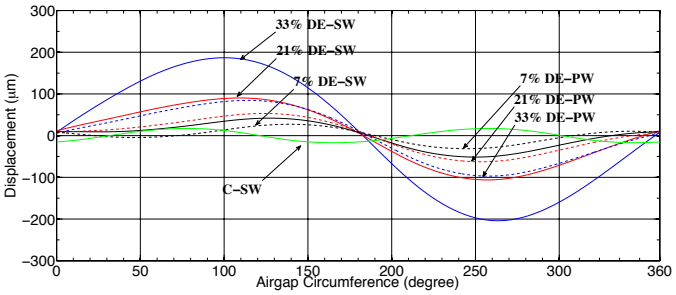

Fig. 13: Stator back iron deflection for different levels of rotor dynamic eccentricities

Level of Eccentricity	Displacement (μm)				Reduction (%)	
	SE-SW	SE-PW	DE-SW	DE-PW	SE-PW	DE-PW
33%	214	73	137	62	34%	45%
21%	125	43	67	38	35%	56%
7%	43	19	29	17	45%	58%

Table 4: The RMS value of deflection obtained from FE modeling for static and dynamic eccentricity

References

[1] McMahon, R., Wang, X., Abdi, E., Tavner, P., Roberts, P., Jagiela, M.: ‘ The BDFM as a generator in wind turbines’ . *Power Electronics and Motion control Conf.*, Portoroz, Slovenia, 2006, pp. 1859– 1865

[2] Tavner, P.J., Higgins, A., Arabian, H., Long, H., Feng, Y.: ‘ Using an FMEA method to compare prospective wind turbine design reliabilities’ . *European wind Energy Conf.* 2010 Technical Track, Warsaw, Poland, April 2010

[3] Polinder, H., van der Pijl, F.F.A., de Vilder, G.-J., Tavner, P.J.: ‘ Comparison of direct-drive and geared generator concepts for wind turbines’ , *IEEE Trans. Energy Convers*., 2006, 21, (3), pp. 725–733

[4] Boger, M., Wallace, A., Spee, R., Li, R.: ‘ General pole number model of the brushless doubly-fed machine’, *IEEE Trans. Ind. Appl.*, 1995, 31, (5), pp. 1022–1028

[5] Carlson, R., Voltolini, H., Runcos, F., Kuo-Peng, P., Baristela, N.: ‘ Performance analysis with power factor compensation of a 75 kW brushless doubly fed induction generator prototype’ . *IEEE Int. Conf. Electric Machines & Drives,* Antalya, Turkey, May 2007, vol. 2, pp. 1502– 1507

[6] Liu, H., Xu, L.: ‘ Design and performance analysis of a doubly excited brushless machine for wind power generator application’ . *IEEE Int. Symp. Power Electronics for Distributed Generation Systems*, Hefei, China, June 2010, pp. 597– 601

[7] Long, T., Shao, S., Abdi, E., et al : ‘ Symmetrical low voltage ride-through of a 250 kW brushless DFIG’. *Sixth IET Int. Conf. Power Electronics, Machines and Drives (PEMD)*, Bristol, UK, March 2012, pp. 1– 6

[8] Seman, S., Niiranen, J., Kanerva, S.: ‘ Performance study of a doubly fed wind-power induction generator under network disturbances’ , *IEEE Trans. Energy Convers.* , 2006, 21 , (4), pp. 883– 890

[9] Shao, S., Abdi, E., McMahon, R.: ‘ Dynamic analysis of the brushless doubly-fed induction generator during symmetrical three-phase voltage dips’ . *Int. Conf. Power Electronics and Drive Systems (PEDS)*, Taipei, Taiwan, November 2009, pp. 464– 469

[10] Boger, M., Wallace, A., Spee, R., Li, R.: ‘ General pole number model of the brushless doubly-fed machine’ , *IEEE Trans. Ind. Appl*., 1995, 31, (5), pp. 1022–1028

[11] A. Burakov and A. Arkkio, “Comparison of the unbalanced magnetic pull mitigation by the parallel paths in the stator and rotor windings,” *IEEE Transactions on Magnetics,* vol. 43, pp. 4083 – 4088, 2007.

[12] D. Dorrell and A. Smith, “Calculation of u.m.p in induction motors with series or parallel winding connections,” *IEEE Transactions on Energy Conversion*, vol. 9, pp. 304 – 310, 1994.

[13] M. DeBortoli, S. Salon, and C. Slavik, “E_ects of rotor eccentricity and parallel windings on induction machine behaviour: A study using finite element analysis,” *IEEE Transactions on Magnetics*, vol. 29, pp. 1676 – 1682, 1993.

[14] D. Zarko, D. Ban, I. Vazdar, and V. Jaric, “Calculation of unbalanced magnetic pull in a salient pole synchronous generator using finite element method and measured shaft orbit,” *IEEE Transactions on Industrial Electronics*, vol. 59, pp. 2536 – 2548, 2012.

[15] J. Li, D. Choi, and Y. Cho, “Analysis of rotor eccentricity in switched reluctance motor with parallel winding using fem,” *IEEE Transactions on Magnetics*, vol. 45, pp. 2851 – 2854, 2009.

[16] D. Dorrell and D. Ionel, “Radial forces and vibrations in permanent magnet and induction machines.” *IEEE Power and Energy Society General Meeting*, 2012, pp. 1 – 6.

[17] F. Runcos, R. Carlson, N. Sadowski, P. Kuo-Peng, and H. Voltolini, “Performance and vibration analysis of a 75 kw brushless doubly-fed induction generator prototype.” *IEEE Industry Application Conference*, 2006, pp. 2395 – 2402.

[18] T. Logan, R. McMahon, and K. Se_en, “Noise and vibration in brushless doubly fed machine and brushless doubly fed reluctance machine,” *IET Electric Power Applications*, vol. 7, pp. 1 – 10, 2014.

[19] D. Dorrell, A. Knight, and R. Betz, “Issues with the design of brushless doubly fed reluctance machines: unbalanced magnetic pull, skew and iron losses,” *IEEE International Electric Machines & Drives Conference (IEMDC)*, pp 663-668, May 2011

[20] R. McMahon, P. Tavner, E. Abdi, P. Malliband, and D. Barker, “Characterising brushless doubly fed machine rotors,” *IET Electric Power Applications*, vol. 7, pp. 535 – 543, 2013.

[21] R. A. McMahon, E. Abdi, P. Malliband, S. Shao, M. E. Mathekga, and P. J. Tavner, “Design and testing of a 250 kw brushless dfig.” Bristol, UK: 6th *IET International Conference on Power Electronics, Machines and Drives (PEMD)*, March 2012.

[22] J. Pyrhonen, T. Jokinen, and V. Hrabovcova, Design of rotating electrical machines. *Finland: John Wiley & Sons Inc*., 2007.

[23] F. Blazquez, C. Veganzones, D. Ramirez, and C. Platero, “Characterization of the rotor magnetic field in a brushless doubly-fed induction machines,” *IEEE Transactions on Energy Conversion*, vol. 24, no. 3, pp. 599 – 607, 2009.